APPLICATION OF THERMOGRAPHY IN ANALYSIS OF FATIGUE STRENGTH OF MATERIALS AND STRUCTURES

*Lovre **KRSTULOVIĆ-OPARA**, Fakultet elektrotehnike, strojarstva i brodogradnje, Sveučilište u Splitu, R. Boškovića 32, HR-21000 Split, www.fesb.hr/kk, lovre.krstulovic-opara@fesb.hr*

ABSTRACT - *Thermography is becoming more and more relevant method in industry and as a research tool. It is an accepted method in many fields where non-destructive testing is carried out. In this paper focus was on evaluation of stress concentrations and fatigue of metal structures. Three thermographic methods: Thermoelastic stress analysis, Risitano method and acquisition of plastification zone and fracture propagation, are addressed and compared with results of classical cyclic testing of Al2024 alloy specimens. Specimens with three types of stress concentrator are used; 3 mm triangular notch, R3 mm circular notch, and a hole with 6 mm diameter. All thermographic methods showed high level of coincidence with classical fatigue tests. Thermoelastic stress analysis provides first stress invariant field for cyclic loaded sample, revealing stress concentrations near notches. Risitano method, from thermal dissipations at various levels of cyclic load, estimates dynamic strength of materials. Fast cooled middle-wave infrared cameras enable locating and tracing material plastification and fracture propagation. The outcomes of all evaluated methods are in accordance with each other.*

Keywords: Thermoelastic stress analysis, Risitano method, plastification, fracture propagation, fatigue, cyclic loading

1. INTRODUCTION

Infrared thermography is nowadays an accepted non-destructive testing (NDT) method. It is applied as passive and active method, as described in our previous work [1-3]. Active thermography is used in NDT of composite polymer materials. Passive thermography is a method used in analysis of materials and structures, e.g. fatigue strength estimation. Passive thermography can also be used in evaluation and detection of plastification and fracture propagation. When used in estimation of fatigue limit it can be considered an NDT method due to the fact that fatigue strength can be estimated without destroying a single specimen.

Fatigue strength estimation is generally based on destructive testing of specimens or whole sections of structure with the goal of predicting the fatigue limit of cyclic loaded structures. Detection and prevention of stress concentrations, as the main source of fracture initialization, is mostly limited to numerical simulations or experimental measurements with methods such as strain gauges, photoelasticimetry, etc. The realistic visualization of structure's stress or strain distribution is hardly achievable with the majority of NDT methods. Strain gauges are applicable for dynamic strain measurements, providing reliable results, but with the drawback of enabling readings only in locations of application. The current development, sensitivity and price of IR thermograpy equipment enabled several thermographic approaches to become popular and accepted as an NDT tool. In the field of dynamic testing the Thermoelastic Stress Analysis (TSA) [3-12] enables a full field visualization of surface stress distribution (the method provides first stress invariant). The estimation of fatigue strength is possible by several passive thermography methods such as Risitano method [13, 14] or Meneghetti method based on energy dissipation [15, 16]. With these methods it is possible to significantly reduce, or completely avoid destruction of test specimens, which reduces the time and cost of fatigue testing.

Lord Kelvin found that elastically deformed bodies generate temperature changes when loading is applied, where tension causes cooling, while compression causes heating. In zones of stress concentrations these effects are more pronounced. For the case of metals, e.g. steel or aluminium, these changes are few milligrades, while for the case of plastic deformations changes are of several grades Celsius. These thermal changes, characterized by significant heat generation, enable detection and estimation of plastification zone propagation, crack propagation or final rupture scenario. The described IR-based methods are applicable to all structural materials, where applicability depends on the surface emission characteristics. Good emission coefficient can always be achieved by the application of high emissivity paint, e.g. Nextel Velvet-Coating 881-21 [17] with emission coefficient of 0.95, Figure 1. In this paper an overview of three methods is given, where the described methods enable visualization of stress distribution, estimation of fatigue limit and detection of plastification or fracture propagation. The obtained results are compared with classical fatigue testing (S-N diagrams). The used specimens are made of aluminium alloy Al2024 with cross section of 20x4 mm and cyclically loaded (r=Fmin/Fmax=0) with loading frequency of 20 Hz. The test specimens are machined with stress concentrators in the form of 6 mm hole, V shape notch (3mm in depth) and semi-circular notch (R3 mm). The cross section of the notched zone is the same for all specimens (14x4 mm).
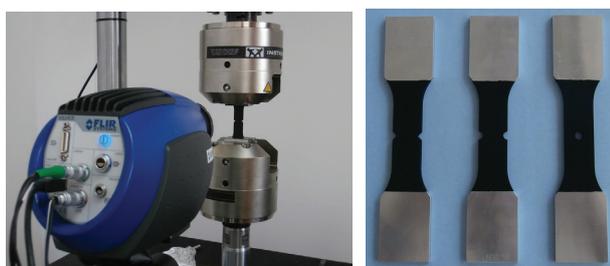
Figure 1 - *Experimental setup and specimens with stress concentrators (V notch, semicircular notch and hole)*

Although all described methods are fully applicable to reinforced polymer composites, only aluminium alloy will be addressed herein. Polymer composites are characterized by significantly lower thermal diffusivity so that the evaluation of such materials is for some of the methods possible even with LW thermal cameras based on micro-bolometric detectors. Due to the high thermal conductivity, high thermal diffusivity and low thermal capacity, metal specimens are characterized by fast thermal changes requiring detection with cooled MW thermal cameras based on photonic detectors. These cooled MW cameras enable acquisition with frame rates of over 700 Hz., where the limit is not due to the technology of detector, but due to the rate of data transfer to computer. Fast cooled MW detectors enable sharp images of dynamic occurrences (20 Hz cyclic loading rate for described examples), which is not the case for micro-bolometric LW detectors. The results presented here are provided by cooled MW camera FLIR SC 5000, with image resolution of 320x256 pixels and sensitivity of 0.02 K. Currently on the market there are similar cameras with double resolution, same sensitivity, but with lower frame rate. For the reduced image size the frame rate is increased up to over 700 Hz. The IC camera used herein, for the full image resolution (320x256 pixels), enabled frame rates of around 150 Hz.

2. EVALUATION OF STRESS DISTRIBUTION BASED ON THERMOELASTICITY

In 1850 Lord Kelvin described the thermoelastic effect based on the fact that the applied load causes thermal changes of objects. In 1915 Compton and Webster conducted the first experimental proof, while in 1967 Belgen provided the first non-contact measurements [18]. With the development of non-contact IR measurement technology method became of particular scientific interest. In 1982 the first images were provided by Ometron SPATE 8000 instrument, where several hours were needed for the acquisition of

stress distribution. The SPATE 8000 was based on a single thermal detector (thermal diode) and set of synchronized moving prisms providing surface thermal scan. In 1994 the introduction of digital focal point array technology enabled by instrument Stress Photonic the stress distribution acquisition within a few minutes.

The TSA method is based on the thermoelastic relation:

$$\Delta T = \frac{-\alpha T}{\rho C_p}(\sigma_1 + \sigma_2) \qquad , \qquad (1)$$

where α is coefficient of thermal expansion, T is room temperature, ρ specimen density, C_p thermal capacity at constant pressure, while σ_1 and σ_2 are principal stresses. Supposing that coefficients α, T, ρ and C_p are constant for the observed specimen, equation (1) provides direct relation between increase in temperature and first stress invariant (the sum of principal stresses, where for the body surfaces 3rd principal stress $\sigma_3=0$). Relation (1) holds for adiabatic condition (no gain or heat loss), which is satisfied for fast load changes (around 10 Hz). Thus, the method requires acquisition with fast cooled MW cameras, cyclic specimen loading of approximately 10 Hz (although loading can be reduced to 3 Hz) and sufficiently high level of stress changes. Load can be generated by magnetic field, ultrasound, or dynamic load actuator as described herein. When acquiring images of a cyclically loaded specimen (Figure 1) at load frequency of 20 Hz, cyclical heat flashes are recorded (Figure 2). In zones of stress concentrations these flashes are stronger. The cyclically loaded specimen in Figure 2 provides images of stress distribution, where cooler zones are zones with higher tensile stresses. As the camera frame rate was set up to 50 Hz (camera system enables higher frame rates), the set of images in Figure 2 demonstrate the problem of capturing the moment of highest loading.
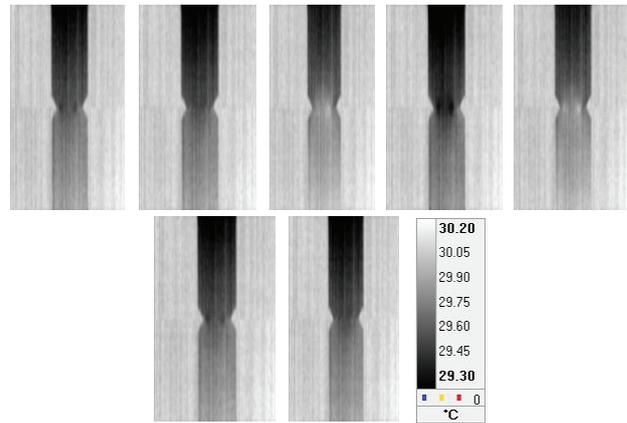
Figure 2 - *Thermal flashes of cyclic loaded specimen (loading frequency of 20 Hz)*

Even when the moment of highest loading is captured, relation (1) will not provide realistic results. To obtain the precise reading of the first stress invariant, an additional hardware component, the so called Lock-In, is required. The Lock-In provides information about applied loading (e.g. the load cell signal) and integrates it with thermal set of images enabling correct stress distribution based on relation (1). Figure 3 illustrates on an example of fillet welded test specimen [19] the difference between raw image and image obtained after Lock-In image processing.
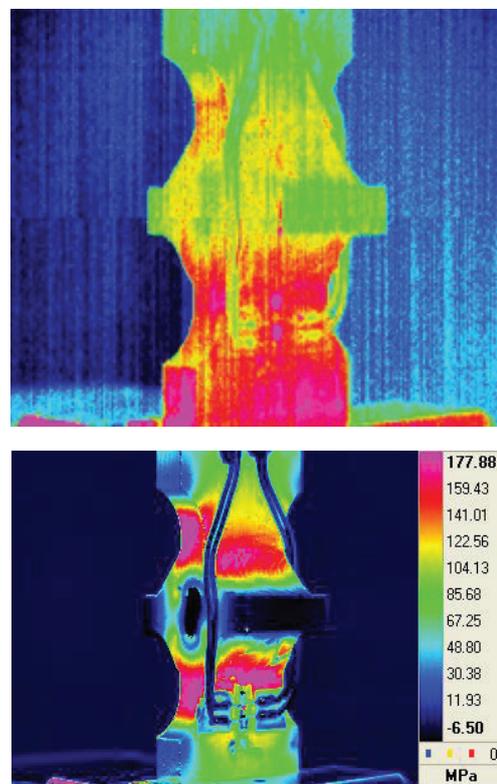
Figure 3 - *Raw image and stress distribution after Lock-In image processing*

Although a very reliable method, the TSA is not so common in literature. The limitations of the method are that cyclic loading is required, the loading must achieve a certain stress level, and the method requires relatively expensive cooled LW camera. The examples of the method are available in references [6, 20-23]. The TSA method is a full field NDT method providing visualization of stress distribution for the whole observed body surface. The method is similar to the method of photoelasticimetry, with the difference in result in the form of the first stress invariant.

3. EVALUATION OF FATIGUE LIMIT BASED ON THE RISITANO METHOD

The Risitano method [13, 14] is based on the fact that at the beginning of cyclic loading, a small increase in specimen's temperature occurs. The increase is stabilized after a few loading cycles, remaining constant until rupture (constant supposing there is no increase in temperatures of the whole experimental setup). A few cycles before rupture, there is significant increase in specimen's temperature, followed by temperature drop after rupture. Figure 4 depicts the increase in temperature during the first load cycles of specimen with V-shaped notch, and sudden increase in temperature for the last loading cycles before rupture (example of 4 kN cyclic loading). This effect is similar to the effect of stress-strain hysteresis that can be observed for the first few loading cycles and the last few cycles before rupture during standard fatigue cyclic test. This hysteresis disappears at the beginning and reappears close to the end of fatigue test. Contrary to classical fatigue test, where several test specimens are needed, the Risitano method enables estimation based on a single test specimen, where final specimen rupture can be avoided. Fatigue limit is estimated from the fact that for a certain amount of load there is no temperature increase. The method is simple and applicable using LW

micro-bolometric cameras. When applied with more sensitive MW cooled cameras, due to the higher acquisition sensitivity, small thermal fluctuations appearing from elastic loading-unloading thermoelastic effect require additional smoothing of temperature data readings. The upper diagram in Figure 5 displays raw temperature data. The lower diagram in Figure 5 displays the smoothed curve that enables easier data evaluation. Thermal fluctuations in the upper diagram are thermal flashes illustrated in Figure 2. LW micro-bolometric cameras do not need such data processing due to the fact that sensitivity and frame rate of such cameras are much lower.
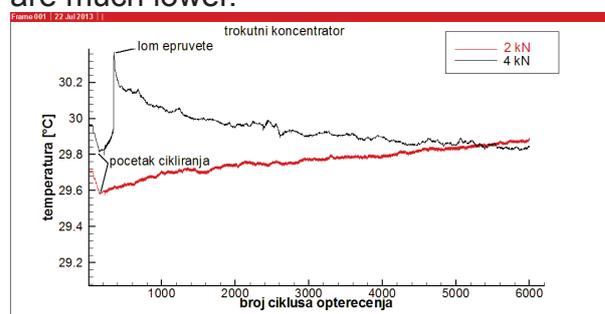
Figure 4 - Increase, stabilization and final increase of specimen's temperature
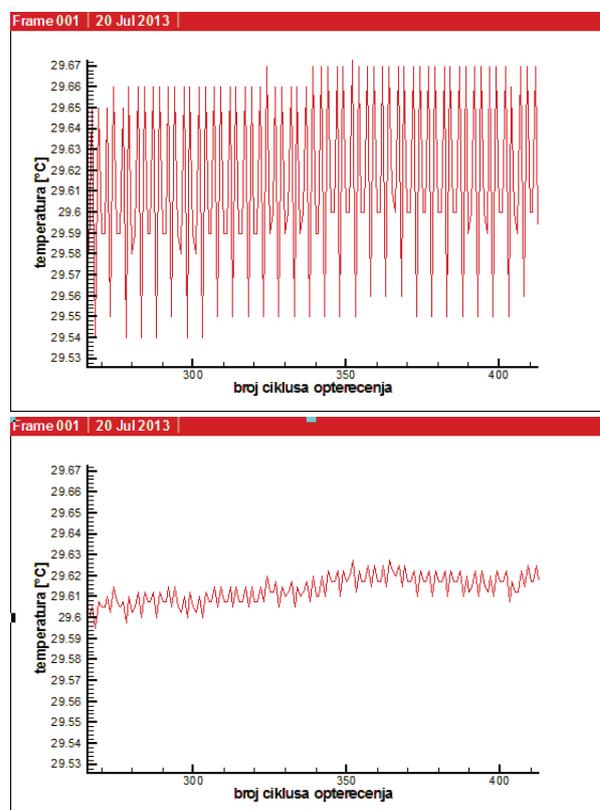
Figure 5 - Thermal fluctuation and smoothed thermal diagram acquired by LW cooled IR camera

4. EVALUATION OF PLASTIFICATION AND RUPTURE PROPAGATION

During elastic cyclic loading tension causes cooling, while compression causes heating of the test specimen according to relation (1). Significant heat generation appearing in zones of yielding enables recording the whole plastification process. Materials with high thermal capacity and low conductivity enable use of LW micro-bolometric cameras. Metals require acquisition with cooled LW cameras. Figures 6-8 depict sequences of plastification initialization, propagation and final rupture. Temperature differences between upper and lower part of specimens are caused by heat flow due to the thermal difference of grips, where lower grip is connected to hot hydraulic piston and the upper one is connected to the cooler load cell.
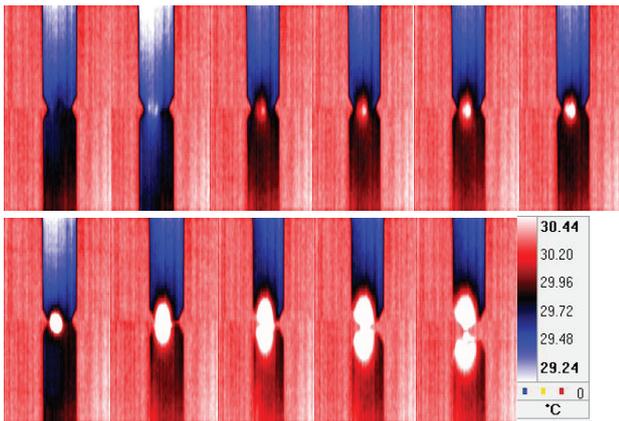
Figure 6 - *Propagation of plastification zone until rupture for V-notched specimen*
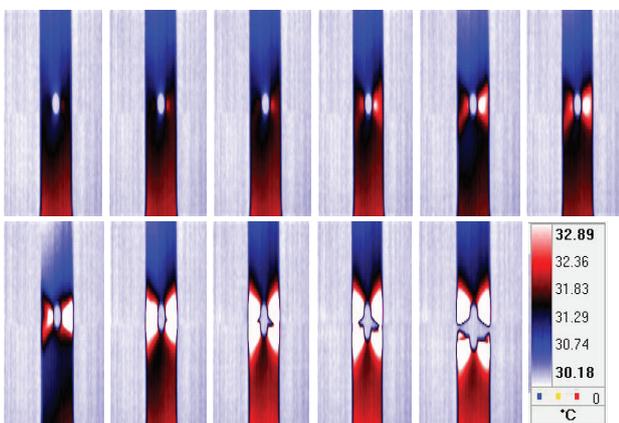
Figure 7 - *Propagation of plastification zone until rupture for specimen with hole*
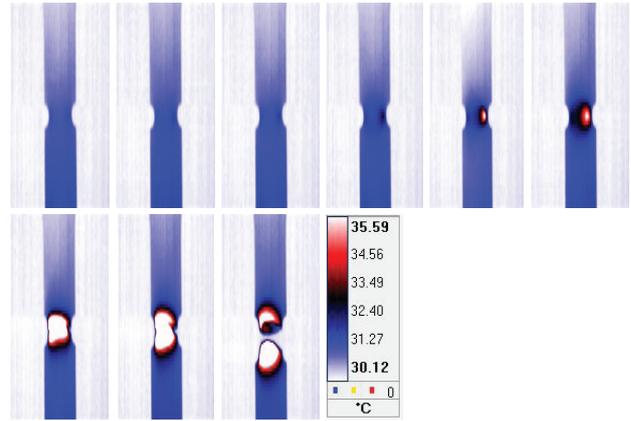
Figure 8 - *Propagation of plastification zone until rupture for specimen with semicircular notch*

5. COMPARISON OF IR-BASED METHODS WITH CLASSICAL CYCLIC FATIGUE TESTS

To demonstrate the capabilities of IR-based methods the obtained results are compared with classical fatigue test for specimens in Figure 1. The S-N diagrams (stress vs. number of cycles) providing relation between the level of sinusoidal cyclic loading and the achieved number of cycles in the logarithmic scale are depicted in Figures 9-11. Symbol "x" in diagrams symbolizes the moment of specimen failure, while the red lines are the mean values for cases where several specimens are loaded with the same cyclic load. Cycling was performed on servo-hydraulic dynamic testing load frame Instron 8800 50 kN at the frequency of 20 Hz. Due to the limited number of available specimens the number of three specimens per each load case has not been achieved. Although partial, S-N diagrams do show material fatigue resistance, making them comparable to the results obtained by addressed IC-based methods.
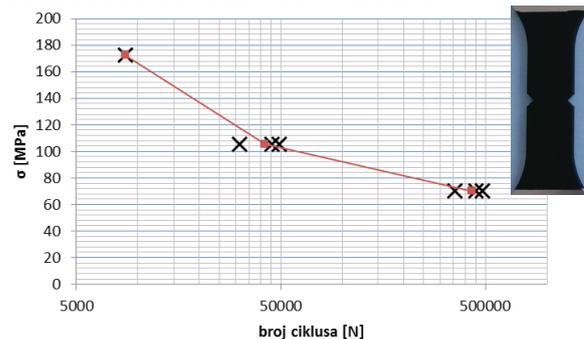
Figure 9 - *S-N diagram for V-shaped notch*
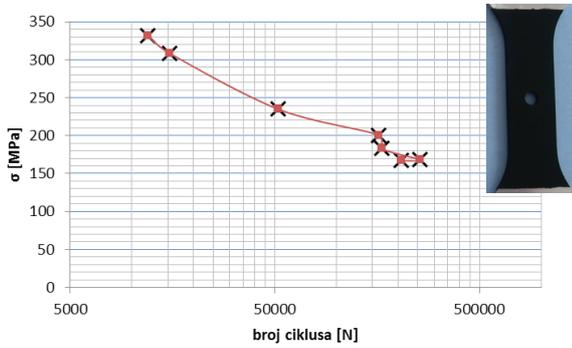
Figure 10 - S-N diagram for specimen with hole
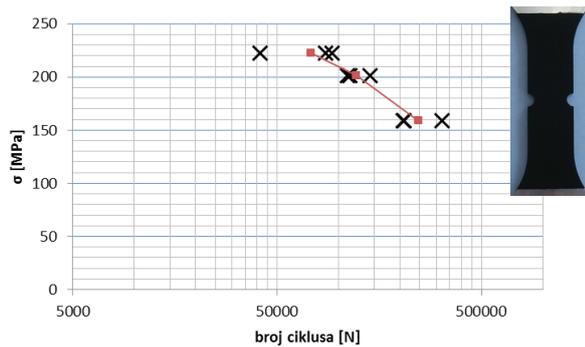
Figure 11 - S-N diagram for semicircular notch

Figure 12 . Stress distribution of V-notched, semicircular notched and specimen with hole at 8 kN cyclic loading

The TSA enables visualization of stress distribution for all analyzed specimens. Figure 12 depicts stress distribution for maximal cyclic load level of 8 kN (corresponds to nominal stress of 143 MPa). Stress scale shows maximal stress appearing for V-shaped notch (94.26 MPa), while semicircular notch has minimal stress, which is comparable to S-N diagrams, where the lowest fatigue resistance characterizes a V-notched specimen. The specimen with hole has slightly lower fatigue resistance than the semicircular notched specimen, which is comparable to maximal stresses in Figure 12 (48.87 MPa for specimen with hole, 42.97 MPa for the semicircular notched specimen).

The thermo elastic effect becomes stronger at higher loadings. Thus, it is not only necessary to achieve the required loading frequency, but the loading level as well. In Figure 13 the stress distribution of V-notched specimen is not displayed as the specimen already ruptured for the loading lower than 16 kN (286 MPa).

Figure 13 - Stress distribution for specimen with hole and semicircular notched specimen at cyclic loading of 16 kN

The Risitano method is based on recording the specimen's temperature for cyclic loaded specimen at different loading levels. Figure 14 depicts the mean temperature of the measured area (blue quadrilateral) for 6,000 cycles of sinusoidal loading at the frequency of 20 Hz. Camera frame rate was set to 50 Hz. Although higher frame rates

are possible, high frame rates will result in unnecessary increase in the collected data. The length of the recorded sequence depends on the temperature stabilization period. In thermal diagrams in Figures 4, 14-17, the thermal drop before the beginning of cycling (Figure 15) is caused by initial tension.
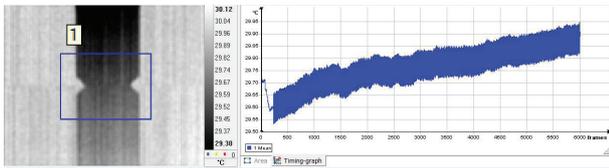
Figure 14 - Time diagram of mean temperature for test area

Thermal diagrams in Figures 15-17 depict thermal increase during 6,000 loading cycles for different load levels at the frequency of 20 Hz, where the ratio of load extremes was r=Fmin/Fmax=0. The initial temperature level depends on the specimen's room temperature and does not influence the method as only relative thermal increase during the test is observed. For each case the thermal increase is higher for higher loading levels. The rupture is characterized by sudden increase in temperature, followed by temperature drop after rupture.
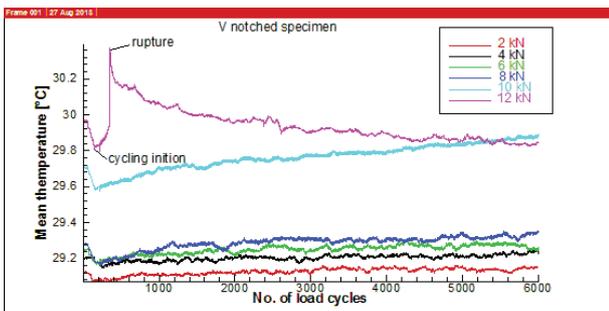
Figure 15 - Time diagram of mean temperature for test area of V-notched specimen
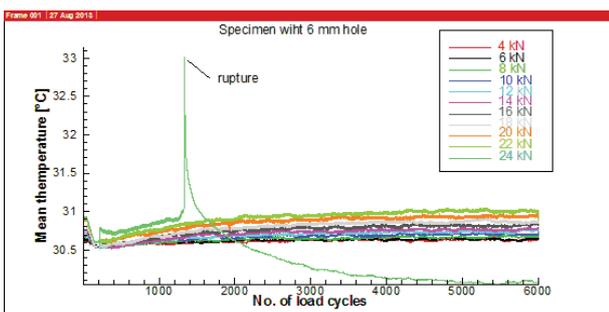
Figure 16 - Time diagram of mean temperature for test area of specimen with 6 mm hole
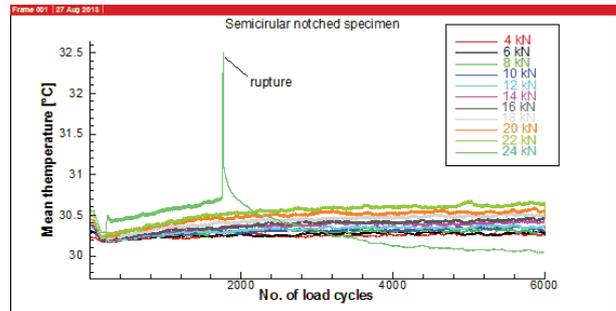
Figure 17 - Time diagram of mean temperature for test area of semicircular notched specimen

Diagrams in Figures 18-20 are thermal increases of mean temperatures displayed in Figures 15-17. At the point where the line defined by linear approximation reaches zero the thermal increase is nominal maximal stress, that is: for V-notched specimen 44 MPa, for specimen with hole 123 MPa, and for semicircular notched specimen 126 MPa. These results correspond to the results of maximal stress obtained by the TSA method at the same level of loading (Figure 12), where maximal stress is observed for V-notched specimen (94 MPa), while for specimen with hole it is 49 MPa, and for semicircular notched specimen it is 43 MPa.

When comparing the results of the Risitano method with the maximal nominal stress in S-N diagrams (Figures 9-11), maximal nominal stresses obtained by the Risitano method correspond to the results obtained in S-N diagrams. As fatigue tests on load frame have not exceeded 10^6 cycles, the obtained results cannot be fully compared, but the trend of stress concentrator influence is clearly visible. To make more precise predictions, reaching 10^7 load cycles is required.
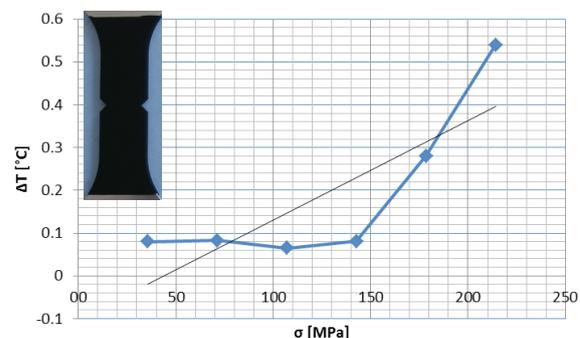
Figure 18 - Thermal increase vs. load level increase and linear approximation of V-notched specimen
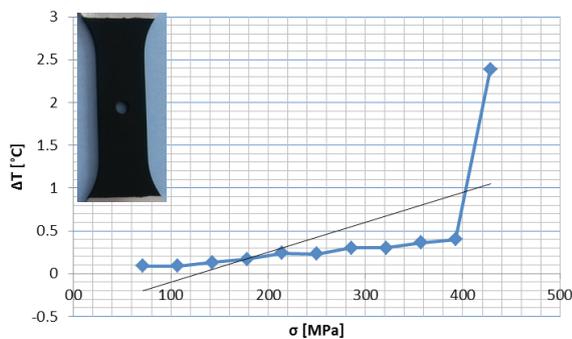
Figure 19 - Thermal increase vs. load level increase and linear approximation of specimen with hole
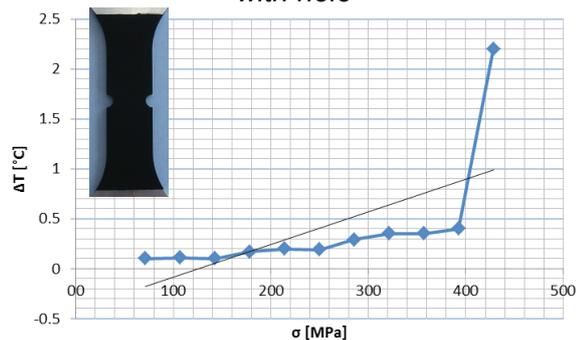
Figure 20 - Thermal increase vs. load level increase and linear approximation of semicircular notched specimen

During the Risitano method testing only three specimens ruptured, which is significantly lower than 23 specimens required for S-N diagrams that did not provide final results of maximal nominal stresses. The testing time required for all specimens evaluated by the Risitano method was several hours, while S-N curves required two weeks of load frame testing.

6. CONCLUDING REMARKS

In this paper an overview of the application of IR-based methods to estimate fatigue resistance, stress concentrations and fatigue strength for metal specimens is presented. All three described methods, i.e. the TSA, the Risitano method and recording of plasticity and crack propagation, are fully applicable on polymer composites. When evaluating metals, i.e. materials with high diffusivity, LW micro-bolometric cameras can only be used in the Risitano method. The TSA requires cooled MW camera, additional Lock-In hardware component, and corresponding data processing software,

which increases the equipment price. These prices have remained constant over the last few years. There have been no significant changes in technology, except that for the same price a camera with double image resolution can be obtained. Double image resolution for the methods addressed here is not necessary, and the increasing image resolution decreases the camera frame rate, which is an important issue. During the last decade several companies that produced MW cameras and image processing software based on Lock-In approach (e.g. Agema, Cedip) have been bought by bigger global companies, mostly oriented towards LW camera market, causing a stagnation of research and applications in the field of TSA. Except for some academic research work, there have been no major steps forward in industrial applications.

This particular area of research and development still enables new approaches and can be of great scientific interest. With regional stagnation in industrial research and development, the research in IR-based methods stagnates as well, which keeps the prices of MW thermal cameras high.

The TSA enables visualization of stress field for object surface, thus enabling the estimation of stress concentrations. When comparing three addressed specimens, it can be concluded that the one with semicircular notch is characterized by the lowest stress concentration and the highest fatigue limit. This has been confirmed by classical fatigue tests, i.e. S-N diagrams. The results obtained by the Risitano method correspond to the results of fatigue tests. Fast cooled MW cameras enable evaluation of plasticity and crack propagation including specimen rupture. These observations can be compared with the TSA, where if the zone of fracture initialization corresponds to stress concentration zones, it proves that the stress concentration is the cause of rupture. If this is not the case, then the cause of rupture can be found in material drawbacks or the machining method.
The TSA, the Risitano method and the acquisition of plastification and fracture

propagation are reliable approaches to estimation of fatigue resistance and stress concentration enabling assessment of materials and structures. The presented methods are dynamic, non-destructive (except fracture propagation) and non-contact methods. The examples demonstrated the ability of IR thermography as a reliable NDT and experimental mechanics tool.

7. References

[1] Krstulović-Opara, L., Domazet, Ž., Klarin, B., Garafulić, E.: The Application of IR Thermography to the NDT and Thermal Stress Analysis, HDKBR info, no. 6/7, 17-22, 2012.

[2] Krstulović-Opara, L., Klarin, B. , Garafulić, E. and Domazet, Ž.: Application of gradient based IR thermography to the GRP structures inspection, Key Engineering Materials, Vols.488-489, 682-685, 2011.

[3] Krstulović-Opara, L. , Klarin, B., Neves, P., Domazet, Ž.: Thermal imaging and Thermoelastic Stress Analysis of impact damage of composite materials, Engineering Failure Analysis, vol. 18, 713–719, 2011.

[4] Lesinak, J.R., Boyce, B.R.: A high-speed differential thermographic camera, SEM conference, 1995.

[5] Lesinak, J.R., Bazile, D.J., Boyce, B.R., Zickel, M.J.: Stress intensity measurement via infrared focal plane array, ASTM conference, May 1996.

[6] Haldorsen, L.M.: Thermoelastic stress analysis system developed for industrial applications, Ph.D. Thesis, University of Aalborg, Institute of mechanical engineering, 1998.

[7] Lesinak, J.R., Boyce, B.R., Howenwater, G.: Thermoelastic measurement under random loading, SEM conference, June 1998.

[8] Boyce, B.R.: Steps to modern thermoelastic stress analysis, ATEM Conference, Ube, Japan, July 1999.

[9] Honlet, M., Boyce, B.R.: Full-field thermoelasticity. A new generation of an optical method showing directly effects produced by mechanical strains, 15th WCNDT, Roma, Italy, 2000.

[10] Dulieu-Barton, J.M., Quinn, S.: Thermoelastic stress analysis of oblique holes in flat plates, Int J Mech Sci, vol. 41, 527–46, 1999.

[11] Boyce, B., Lesniak, J.: Unique applications of thermoelastic stress analysis, Spring SEM conference, 1999.

[12] Lesniak J, Bartel B.: An elevated-temperature TSA furnace design, Exp Techniques, 20(2):96, 1999

[13] La Rosa, G., Risitano, A.: Thermographic methodology for rapid determination of the fatigue limit of materials and mechanical components, International Journal of Fatigue, vol. 22, 65-73, 2000.

[14] Fargione, G., Geraci, A., La Rosa, G., Risitano, A.: Rapid determination of the fatigue curve by the thermographic method, International Journal of Fatigue, vol. 24, 11-19, 2002.

[15] Meneghetti, G.: Analysis of the fatigue strength of a stainless steel based on the energy dissipation, International Journal of Fatigue, vol. 29, 81-94, 2007.

[16] Minak, G.: On the Determination of the Fatigue Life of Laminated Graphite-Epoxy Composite by Means of Temperature Measurement, Journal of Composite Material, vol. 44, 2010.

[17] Tang-Kwor, E., Matteï, S.: Emissivity measurements for Nextel Velvet Coating 811-21 between -36 °C and 82 °C., High Temp.-High Press., vol. 33, 551-556, 2001.

[18] Boyce, B.R.: Steps to Modern Thermoelastic Stress Analysis, ATEM Conference, July 1999, Ube, Japan,1999.

[19] Pirsić, T. , Krstulović-Opara, L , Domazet, Ž.: Thermographic Analysis of Stress Distribution in Welded Joints, The European physical journal. EPJ Web of Conferences, 6, 07004-p1 - 07004-p6, 2010.

[20] Medgenber, J., Ummenhofer, T.: Assessment fatigue damage in low-carbon steel using lock-in thermography, 8th Int. Conference on Quantitative infrared Thermography (QUIRT 2006), June 28-29, Padova, Italy, 2006.

[21] Lin, S.-J., Quinn, S., Matthys, D.R., New, A.M., Kincaid, I.M., Boyce, B.R., Khaja, A.A., Rowlands, R.E.: Thermoelastic Determination of Individual Stresses in Vicinity of a Near-Edge Hole Beneath a Concentrated Load, Experimental Mechanics, vol. 51, 797-814, 2011.

[22] Cavaliere, P., Rossi, G.L., Di Sante, R., Moretti, M.: Thermoplasticity for the evaluation of fatigue behavior of 7005/Al2O310p metal matrix composite sheets joined by FSW, International Journal for Fatigue, vol. 30, 198-206, 2008.

[23] Lesinak, J.R., Boyce, B.R.: A High-Speed Differential Thermographic Camera, SEM Conference, 1995.